SCIENCE CHINA
Physics, Mechanics & Astronomy

•Article•

September 2020 Vol. 63 No. 9: 297011
https://doi.org/10.1007/s11433-019-1508-2

Surface protonation and oxygen evolution activity of epitaxial $La_{1-x}Sr_xCoO_3$ thin films

XiaoShuo Wang[1], Liang Zhou[2], MengXin Li[1], Yi Luo[2], TieYing Yang[3], TianLi Wu[1], XiaoLong Li[3], Kui-Juan Jin[4], Er-Jia Guo[4,5], LiFen Wang[4], XueDong Bai[4], WeiFeng Zhang[1*], and HaiZhong Guo[2,6*]

[1] *Henan Key Laboratory of Photovoltaic Materials, School of Physics and Electronics, Henan University, Kaifeng 475004, China;*
[2] *School of Physics and Microelectronics, Zhengzhou University, Zhengzhou 450001, China;*
[3] *Shanghai Synchrotron Radiation Facility (SSRF), Shanghai Institute of Applied Physics, Chinese Academy of Sciences, Shanghai 201204, China;*
[4] *Beijing National Laboratory for Condensed Matter Physics, Institute of Physics, Chinese Academy of Sciences, Beijing 100190, China;*
[5] *Center of Materials Science and Optoelectronics Engineering, University of Chinese Academy of Sciences, Beijing 100049, China;*
[6] *Collaborative Innovation Center of Light Manipulations and Applications, Shandong Normal University, Jinan 250358, China*

Received November 23, 2019; accepted January 7, 2020; published online May 9, 2020

As an alternative electrode material, transition metal oxides are promising candidates due to multivalent nature and oxygen vacancies present in the structure with facilitate redox reactions. The aim of this study is to explore the intrinsic mechanism of oxygen evolution reaction (OER) using two-dimensional thin film $La_{1-x}Sr_xCoO_3$ electrode as a model. Herein, we report a planar two-dimensional model $La_{1-x}Sr_xCoO_3$ electrode grown on a Nb-$SrTiO_3$ single-crystal substrate via pulsed laser deposition. The two-dimensional $La_{1-x}Sr_xCoO_3$ films offer different oxygen evolution activities at different pH electrolyte solutions. The mechanisms behind the variations of the oxygen evolution activity were discussed after comparing the oxygen evolution activity before and after treatments of the electrodes and measurements by various test methods. The results of this study offer a promising, low-cost electrode material for the efficient OER and a sustainable production of hydrogen fuel.

oxygen evolution reaction, $La_{1-x}Sr_xCoO_3$ thin films, lattice oxygen protonation

PACS number(s): 82.45.Jn, 73.90.+f, 82.65.+r

Citation: X. S. Wang, L. Zhou, M. X. Li, Y. Luo, T. Y. Yang, T. L. Wu, X. L. Li, K.-J. Jin, E.-J. Guo, L. F. Wang, X. D. Bai, W. F. Zhang, and H. Z. Guo, Surface protonation and oxygen evolution activity of epitaxial $La_{1-x}Sr_xCoO_3$ thin films, Sci. China-Phys. Mech. Astron. **63**, 297011 (2020), https://doi.org/10.1007/s11433-019-1508-2

1 Introduction

The growing population and technological development rapidly increase energy consumption worldwide, and the use of non-renewable sources puts pressure on the sustainability of environment. Therefore, new sources of sustainable and environmentally friendly energy are necessary. Hydrogen, as a green energy source, is a promising alternative to fossil fuels and can be produced through the electrolysis of water [1]. The electrolysis of water can be represented by two half-reactions: oxygen evolution reaction (OER) at the anode and hydrogen evolution reaction at the cathode. By comparing the kinetics of two processes, it is determined that OER is a slower process and requires the use of highly active and

*Corresponding authors (WeiFeng Zhang, email: wfzhang6@163.com; HaiZhong Guo, email: hguo@zzu.edu.cn)

noble metal-based catalysts. The high over-potential for O_2 evolution requires the application of high voltages for the efficient electrolysis of water, which limits the practical application of water electrolysis for the production of hydrogen gas. Therefore, the development of highly efficient catalysts for OER that are based on more abundant and non-noble metals has been an intensely studied research topic in the past decade. To develop such catalysts, it is necessary to understand the underlying mechanism of the OER catalysis and determine correlations with structural properties such as transition metal substitution [2,3], oxygen vacancies [4,5], and stress interaction [6-8].

The valence state of transition metals in corresponding oxides is essential for many physical properties of such materials and their practical applications. Specifically, the multivalent nature of transition metal oxides allows it to form oxygen vacancies in the solid state structure, which facilitates the redox reaction [9]. It has been previously shown that the control of *d*-band electron population and spin configuration is crucial for the production of improved transition metal oxide-based electrodes [2,10].

Owing to the multiple valence state, rich phase diagram, and high oxygen mobility, the Co-based oxides represent the promising electrode materials for the reversible redox activity in OER [11-13]. Among them, $LaCoO_3$ is most commonly studied as the electrode material. The material is commonly doped with strontium, which creates the $La_{1-x}Sr_xCoO_3$ powder with the improved electrocatalytic performance [1,14]. However, there are few reports on the thin-film $La_{1-x}Sr_xCoO_3$ electrodes for OER [15,16].

The epitaxial technology allows thin films to be formed with a highly ordered crystalline structure. Recent developments in this field allow the transition metal oxide layers to be formed with controllable structural properties, which promote the structural and mechanistic studies on various physical and chemical properties [17-19]. Several studies have reported the use of epitaxial thin films as working electrodes [20,21]. Therefore, the epitaxial thin-film electrodes made of transition metal oxides are the promising candidates for studying the mechanism of the OER process during the electrolysis of water. The ordered 2D structure of the epitaxial film electrode surface provides a limited and controllable area where electrode reaction occurs, which simplifies the study on a mechanism of electrode reactions during the electrolysis of water. Therefore, any structural changes caused by the electrochemical reaction can be easily detected on the flat surface of the epitaxial thin film [22,23].

In this study, several $La_{1-x}Sr_xCoO_3$ single-crystal thin films were synthesized by pulsed laser deposition and investigated as the electrode material for OER. The amount of the Sr dopant was optimized to provide the best electrochemical performance. The optimized material was used as a working electrode to study the OER activity at different pH values of the solution. The mechanism of OER at different surface protonation states was discussed.

2 Experiment

Epitaxial $La_{1-x}Sr_xCoO_3$ (x=0.0, 0.1, 0.2, 0.3, 0.4, and 0.5) thin films were deposited on single-crystal Nb-$SrTiO_3$ (N-STO, (001)-oriented) substrates (5 mm×5 mm×0.5 mm) using the pulsed laser technique (KrF laser, 1.5 J/cm^2, 248 nm, 2 Hz) at 750°C and the O_2 partial pressure of 5 Pa. Then, *in situ* annealing was conducted for 30 min followed by cooling to room temperature (15°C/min).

To fabricate the working electrode, Cu wire was connected to the N-STO substrate using silver paint, and the edges of the sample were protected using a non-conductive epoxy resin, and only the $La_{1-x}Sr_xCoO_3$ films were in contact with the solution. The standard and three-electrode electrochemical cell was used to measure the OER activity of the working electrode. The Hg/HgO electrode was used as a reference, and Pt wire was used as a counter electrode. The working electrode was analyzed in the solutions with different pH values; these solutions were obtained by dissolving p.a. KOH in deionized water (18.2 MΩ·cm^{-1}). The initial cyclic voltammetry (CV) was studied in the O_2-saturated electrolyte at a 100 mV/s scan rate. The OER activity of the working electrode was determined in the O_2-saturated electrolyte in the voltage range between 1.35 V and 1.75 V (vs. RHE) at 10 mV/s to reduce the capacitance current. The average of forward and backward CV scans yielded the capacitance-free CV curve.

3 Results and discussion

The crystal structure of $La_{1-x}Sr_xCoO_3$ films was determined by an X-ray diffractometer (XRD) with a Cu Kα radiation source (λ = 0.154145 nm) in the θ-2θ mode. The structure of $La_{0.7}$-$Sr_{0.3}CoO_3$ thin films was characterized using Synchrotron X-ray diffraction (SXRD) at the BL14B1 beamline of Shanghai Synchrotron Radiation Facility, using 1.24 Å X-ray source and a Huber 5021 six-axis diffractometer. The structure of the $La_{0.7}Sr_{0.3}CoO_3$ thin films was visualized using the high-angle annular dark-field (HAADF) scanning transmission electron microscopy (STEM) technique on ARM-200F STEM (JEOL, Tokyo, Japan) operating at 200 kV. The surface properties of $La_{0.7}Sr_{0.3}CoO_3$ thin films were characterized using atomic force microscopy (AFM, Bruker multimode 8.0).

The XRD patterns of $La_{1-x}Sr_xCoO_3$ thin films (x=0, 0.1, 0.2, 0.3, 0.4, and 0.5) are shown in Figure S1. Besides the N-STO substrate peaks, only (001) plane reflection peaks from $La_{1-x}Sr_xCoO_3$ films were observed, which indicated the

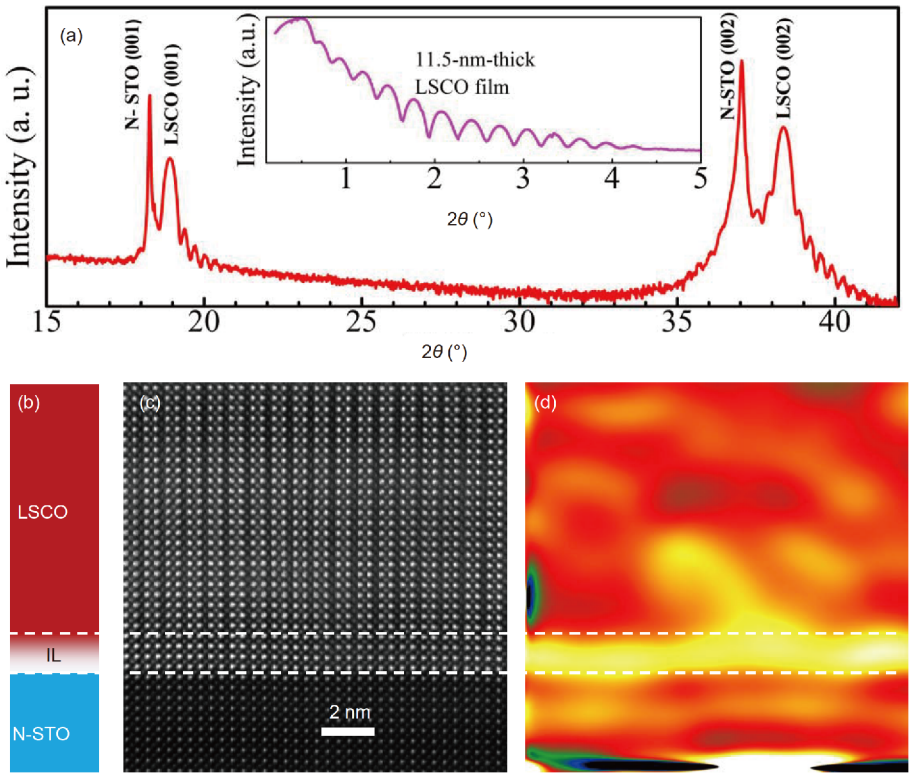

Figure 1 (Color online) (a) SXRD θ-2θ scan curve of the $LaSr_{0.3}Co_{0.7}O_3$ thin film. Inset: X-ray reflectivity profile; (b) geometry of $LaSr_{0.3}Co_{0.7}O_3$; (c) HAADF image of the $LaSr_{0.3}Co_{0.7}O_3$ film. The image was acquired along the [100] zone axis. (d) Geometric phase analysis image.

presence of single phase *c*-axis-oriented thin films. The typical reflectivity profile of the $La_{0.7}Sr_{0.3}CoO_3$ thin film is shown as an inset in Figure 1(a); interference (Kiessig) fringes can be also observed. The film thickness of approximately 11.5 nm was calculated by fitting the periodicity of Kiessig fringes.

The geometrical characteristics of the $La_{0.7}Sr_{0.3}CoO_3$ thin film deposited on N-STO are shown in Figure 1(b), which indicates the presence of interfacial region with an approximately 4-unit-cell thickness. The HAADF-STEM image (Figure 1(c)) provides additional insight about the characteristics of the interfacial region. It is observed that the unit cells of the $La_{0.7}Sr_{0.3}CoO_3$ film and N-STO substrate create a coherent interface without any evidence of mismatches in the (001) plane. In addition, the geometrical phase analysis shown in Figure 1(d) confirms the presence of a 4-unit-cell thick interfacial region with large strain and no mismatches. The film has an in-plane lattice constant that is identical to the substrate when averaging over 3-4 atomic planes [24]. The surface morphology analysis by AFM (Figure S2) identified the root mean square film roughness of (0.56 ± 0.03) nm, which indicated the good surface microstructure of $La_{0.7}Sr_{0.3}CoO_3$.

The OER activity of $La_{1-x}Sr_xCoO_3$ ($0 \le x \le 0.5$) epitaxial films was characterized using CV. As can be seen from Figures 2 and S3, the best catalytic activity was obtained for the $La_{1-x}Sr_xCoO_3$ electrode with x=0.3 ($La_{0.7}Sr_{0.3}CoO_3$). Therefore, $La_{0.7}Sr_{0.3}CoO_3$ was selected for further structural and mechanistic investigations of the OER activity.

The OER activity of the $La_{0.7}Sr_{0.3}CoO_3$ epitaxial film electrode in KOH solutions with different pH values with different times (0-9 h) was studied by CV, as shown in Figure 3(a)-(d). The pH-dependence of $La_{0.7}Sr_{0.3}CoO_3$ shown in Figure S4(a) clearly indicates that the OER activity increases with an increase of pH. This result is consistent with the previous report [25]. The cyclovoltammograms of $La_{0.7}Sr_{0.3}CoO_3$/N-STO and pristine N-STO in the 0.1 mol/L KOH (pH=13) solution saturated with O_2 recorded with a 10 mV/s scan rate are shown in Figure S4(b), confirming that the OER activity comes from $La_{0.7}Sr_{0.3}CoO_3$. On the basis of the changes in the OER activity, the importance of lattice O atoms in the OER mechanism of $La_{0.7}Sr_{0.3}CoO_3$ is confirmed and rationalized using the traditional proton-coupled electron transfer mechanism. Therefore, the proposed mechanism of the OER activity includes lattice O atoms [25].

Figure S5 shows the put-of-plane XRD spectral data of the $La_{0.7}Sr_{0.3}CoO_3$ films soaked in the solutions at different pH. The characteristic diffraction peaks of the (002) plane shifts to the lower angles with an increase of pH from 7 to 11, which suggests the expansion of the lattice in out-of-plane directions. Such shifts were not observed at pH=13.

To further characterize the surface of $La_{0.7}Sr_{0.3}CoO_3$/Nb-

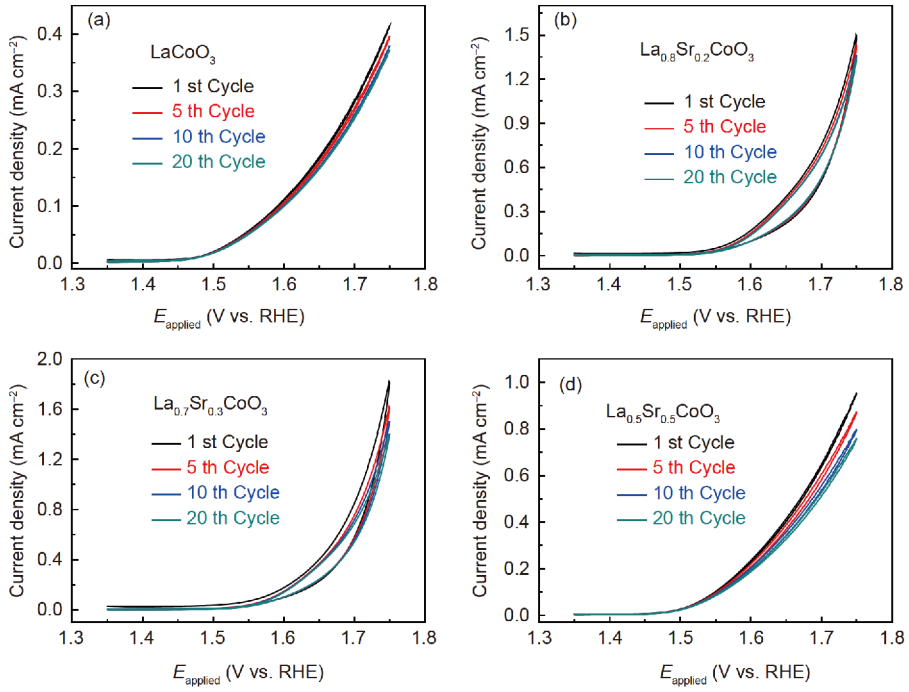

Figure 2 (Color online) Cyclic voltammograms of (a) $LaCoO_3$; (b) $La_{0.8}Sr_{0.2}CoO_3$; (c) $La_{0.7}Sr_{0.3}CoO_3$; and (d) $La_{0.5}Sr_{0.5}CoO_3$, showing the 1st, 5th, 10th, and 20th cycle. All electrodes were cycled 5 times from 1.35 to 1.75 V (vs. RHE) at 10 mV/s in the O_2-saturated 1 mol/L KOH electrolyte.

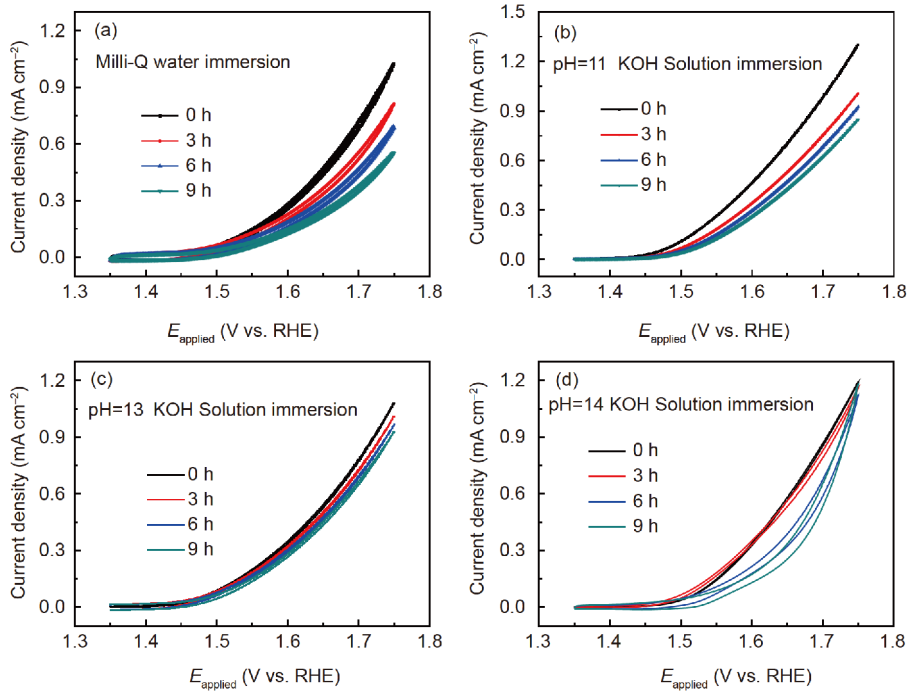

Figure 3 (Color online) CV measurements after the treatment with (a) Milli Q water and (b) potassium hydroxide solution at pH 11; (c) pH 13; and (d) pH 14 for different amounts of time.

STO, we recorded the XPS spectra after soaking the electrode in solutions with pH=7 or pH=13 for 6 h. The changes in oxygen concentration on the surface of the electrode before and after protonation were monitored through the changes in the characteristic O 1s region (Figure S6). The XPS spectra were deconvoluted into three Gaussian curves, which correspond to free water (H_2O), protonated oxygen (M–OH), and oxygen in the bulk solid phase (M–O–M). The

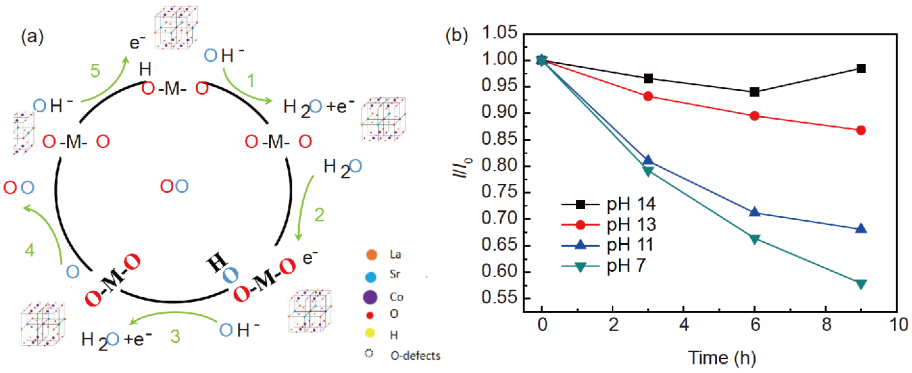

Figure 4 (Color online) (a) Reaction mechanism diagram of lattice oxygen protonation; (b) specific OER activity (current normalized by the oxide BET surface area) at 1.75 V vs. the RHE correction as a function of pH.

changes in M–O–M, M–OH, and H_2O peak areas normalized by the sum of M–O–M and M–OH were measured. The (M–O–M)/(M–O–M+M–OH) ratios for untreated, pH=7, and pH=13 samples were 0.56, 0.45, and 0.54, respectively. We concluded that the alkaline treatment of surface did not change the surface properties of the film compared to the untreated sample.

The results shown in Figure S6 reveal that the degree of surface protonation at pH above 13 is the same as that for the untreated sample. However, thin film becomes highly protonated when it is immersed in pure water (pH=7). With an increase in the degree of protonation of the surface, the OER activity decreases, which suggests the important role of deprotonated lattice O atoms in the mechanism of OER. The important role of lattice O in the OER mechanism is confirmed experimentally on the basis of the changes in the OER activity with an increase of pH. The plausible reaction mechanism is illustrated in Figure 4(a) [25]. Compared to the traditional proton-coupled electron transfer mechanism, this mechanism better explains the pH-dependent oxygen evolution activity of the electrodes. The treatment of electrodes with the solutions at different pH modifies the catalytic activity; the proposed mechanism rationalizes the effect of protonation on the oxygen evolution activity of the electrode. The ratio of current density of the $La_{0.7}Sr_{0.3}CoO_3$ working electrode at different pH values and constant potential applied (U_{RHE}=1.75 V) is shown in Figure 4(b). The improved OER activity with an increase of the pH values is clearly observed. These results confirm the inhibiting effect of the $La_{0.7}Sr_{0.3}CoO_3$ surface protonation on the OER activity.

4 Conclusion

In this study, the oxygen evolution activity of the epitaxial $La_{0.7}Sr_{0.3}CoO_3$ thin-film electrode was investigated at different pH values using CV, XRD, XPS, and STEM techniques. The OER activity of the LSCO electrode is directly proportional to pH, which indicates the importance of surface deprotonation on the OER reaction mechanism. The degree of protonation of lattice oxygen in the aqueous solution slightly changes at pH=13, and the effect of a further increase of pH on the OER activity is negligible. The presence of non-protonated lattice O atoms determines the catalytic activity of the LSCO electrode.

This work was supported by the National Natural Science Foundation of China (Grant Nos. 11574365, and 11974099), and the Program for the Innovation Team of Science and Technology in University of Henan (Grant No. 20IRTSTHN014). The authors thank the beam line BL14B1 (Shanghai Synchrotron Radiation Facility) for providing the beam time and helps during experiments.

Supporting Information

The supporting information is available online at phys.scichina.com and http://link.springer.com/journal/11433. The supporting materials are published as submitted, without typesetting or editing. The responsibility for scientific accuracy and content remains entirely with the authors.

1 X. Cheng, E. Fabbri, M. Nachtegaal, I. E. Castelli, M. El Kazzi, R. Haumont, N. Marzari, and T. J. Schmidt, Chem. Mater. **27**, 7662 (2015).
2 J. Suntivich, K. J. May, H. A. Gasteiger, J. B. Goodenough, and Y. Shao-Horn, Science **334**, 1383 (2011).
3 S. Klaus, Y. Cai, M. W. Louie, L. Trotochaud, and A. T. Bell, J. Phys. Chem. C **119**, 7243 (2015).
4 A. Grimaud, K. J. May, C. E. Carlton, Y. L. Lee, M. Risch, W. T. Hong, J. Zhou, and Y. Shao-Horn, Nat. Commun. **4**, 2439 (2013).
5 N. Lu, P. Zhang, Q. Zhang, R. Qiao, Q. He, H. B. Li, Y. Wang, J. Guo, D. Zhang, Z. Duan, Z. Li, M. Wang, S. Yang, M. Yan, E. Arenholz, S. Zhou, W. Yang, L. Gu, C. W. Nan, J. Wu, Y. Tokura, and P. Yu, Nature **546**, 124 (2017).
6 Y. Liang, Y. Li, H. Wang, and H. Dai, J. Am. Chem. Soc. **135**, 2013 (2013).
7 M. Gong, Y. Li, H. Wang, Y. Liang, J. Z. Wu, J. Zhou, J. Wang, T. Regier, F. Wei, and H. Dai, J. Am. Chem. Soc. **135**, 8452 (2013).
8 Y. Gorlin, C. J. Chung, J. D. Benck, D. Nordlund, L. Seitz, T. C. Weng, D. Sokaras, B. M. Clemens, and T. F. Jaramillo, J. Am. Chem. Soc. **136**, 4920 (2014).
9 T. Ishihara, *Perovskite Oxide for Solid Oxide Fuel Cells* (Springer, New York, 2009), p.43.

10 J. Suntivich, H. A. Gasteiger, N. Yabuuchi, H. Nakanishi, J. B. Goodenough, and Y. Shao-Horn, Nat. Chem. **3**, 546 (2011).
11 H. Jeen, W. S. Choi, M. D. Biegalski, C. M. Folkman, I. C. Tung, D. D. Fong, J. W. Freeland, D. Shin, H. Ohta, M. F. Chisholm, and H. N. Lee, Nat. Mater. **12**, 1057 (2013), arXiv: 1308.5602.
12 J. Zhao, Y. Luo, J. O. Wang, H. Qian, C. Liu, X. He, Q. Zhang, H. Huang, B. Zhang, S. Li, E. Guo, C. Ge, T. Yang, X. Li, M. He, L. Gu, K. J. Jin, K. Ibrahim, and H. Guo, Sci. China Mater. **62**, 1162 (2019).
13 J. Zhao, H. Guo, X. He, Q. Zhang, L. Gu, X. Li, K. Jin, T. Yang, C. Ge, Y. Luo, M. He, Y. Long, J. Wang, H. Qian, C. Wang, H. Lu, G. Yang, and K. Ibrahim, ACS Appl. Mater. Interfaces **10**, 10211 (2018).
14 K. J. May, C. E. Carlton, K. A. Stoerzinger, M. Risch, J. Suntivich, Y. L. Lee, A. Grimaud, and Y. Shao-Horn, J. Phys. Chem. Lett. **3**, 3264 (2012).
15 M. Komo, A. Hagiwara, S. Taminato, M. Hirayama, and R. Kanno, Electrochemistry **80**, 834 (2012).
16 Y. Miyahara, K. Miyazaki, T. Fukutsuka, and T. Abe, ChemElectroChem **3**, 214 (2015).
17 L. F. Wang, Y. Luo, J. S. Wang, X. S. Huang, Z. M. Gao, T. Y. Yang, X. L. Li, P. Li, K. J. Jin, W. F. Zhang, and H. Z. Guo, Sci. China-Phys. Mech. Astron. **62**, 987721 (2019).
18 H. K. Song, K. Xia, and J. Xiao, Sci. China-Phys. Mech. Astron. **61**, 107011 (2018).
19 D. C. Yuan, J. L. Wang, N. Fu, X. L. Wu, Y. J. Ma, and S. F. Wang, Sci. China-Phys. Mech. Astron. **61**, 107321 (2018).
20 R. Tang, Y. Nie, J. K. Kawasaki, D. Y. Kuo, G. Petretto, G. Hautier, G. M. Rignanese, K. M. Shen, D. G. Schlom, and J. Suntivich, J. Mater. Chem. A **4**, 6831 (2016).
21 L. Wang, K. A. Stoerzinger, L. Chang, J. Zhao, Y. Li, C. S. Tang, X. Yin, M. E. Bowden, Z. Yang, H. Guo, L. You, R. Guo, J. Wang, K. Ibrahim, J. Chen, A. Rusydi, J. Wang, S. A. Chambers, and Y. Du, Adv. Funct. Mater. **28**, 1803712 (2018).
22 K. A. Stoerzinger, W. T. Hong, X. R. Wang, R. R. Rao, S. B. Subramanyam, C. Li, C. Ariando, T. Venkatesan, Q. Liu, E. J. Crumlin, K. K. Varanasi, and Y. Shao-Horn, Chem. Mater. **29**, 9990 (2017).
23 K. A. Stoerzinger, M. Risch, J. Suntivich, W. M. Lü, J. Zhou, M. D. Biegalski, H. M. Christen, H. M. Ariando, T. Venkatesan, and Y. Shao-Horn, Energy Environ. Sci. **6**, 1582 (2013).
24 Q. Van Overmeere, J. D. Baniecki, T. Yamazaki, D. Ricinschi, H. Aso, Y. Miyata, H. Yamada, N. Fujimura, Y. Kataoka, and Y. Imanaka, Appl. Phys. Lett. **106**, 241602 (2015).
25 A. Grimaud, O. Diaz-Morales, B. Han, W. T. Hong, Y. L. Lee, L. Giordano, K. A. Stoerzinger, M. T. M. Koper, and Y. Shao-Horn, Nat. Chem. **9**, 457 (2017).